Mechanistic Studies of Adamantylacetophenones with Competing Reaction Pathways in Solution and in the Crystalline Solid State

Vince M. Hipwell and Miguel A. Garcia-Garibay*

Department of Chemistry and Biochemistry, University of California, Los Angeles, California 90095-1569, United States

*email: mgg@chem.ucla.edu

ABSTRACT: Photochemical reactions in crystals occur under conditions of highly restricted molecular mobility such that only one product is generally obtained, even when there are many others that can be observed in the gas phase or in solution. A series of 2-(1-adamantyl)-*ortho*-alkyl-acetophenones with gamma hydrogen atoms on both the adamantyl and *ortho*-aromatic groups was selected to determine whether or not one can engineer and observe competing Norrish Type II reaction pathways in the crystalline state. It was shown that excited state competition for hydrogen abstraction between secondary adamantyl and benzylic hydrogens is affected not only by the relative bond dissociation energies but also by the molecular conformation in the crystal. The subsequent fate of the resulting biradical species is determined by competition between radical recombination to form photoproduct and reverse hydrogen atom transfer to regenerate the starting ketone. Crystallographic information, photoproduct distributions in solution and in the solid state, and the results of multiple mechanistic experiments including transient absorption spectroscopy in acetonitrile and with nanocrystals suspended in water are reported. The results demonstrate that it is possible to engineer competing reactions in crystals and that consideration of all of the aforementioned factors is necessary in order to account for the observed photoproduct selectivity.

INTRODUCTION

The Norrish Type II reaction is one of the most widely studied photochemical processes, and many mechanistic studies have been reported on a broad range of compounds both in solution and in the solid state.[1–6] In a recent study, crystals of adamantyl-*para*-methoxy-acetophenone (**1**, Figure 1) were utilized for one of the first mechanistic investigations of the Norrish Type II reaction based on absolute photochemical kinetics in the solid state using laser flash photolysis (LFP) of aqueous nanocrystalline suspensions.[7] Along with the identification of transient intermediates and their lifetimes, it was shown that the photoproduct diastereoselectivity for **1** is affected by the rotation of the globular adamantane group, which occurs in both solution and the solid state. Given this interesting result, we decided to use the adamantylacetophenone structure as a platform for further investigation of the Norrish Type II reaction. In particular, we sought to probe the reaction mechanism and product selectivity for compounds designed to facilitate multiple hydrogen transfer pathways such that reactivity trends and product selectivity factors may be elucidated.

Modifications of the structure **1** to include *ortho*-alkyl substituents to the acetophenone chromophore provides an opportunity for competition between two analogous photochemical reaction pathways in the *ortho*-aryl substituted adamantylacetophenones **2-5** (Figure 1). There is one set of abstractable gamma hydrogens on the adamantyl group, shown in blue for compounds **1** and **2**, and another one on the *ortho*-alkyl groups in the case of **2-4**, which are shown in red for compound **2**. The latter structures contain chemodiv-

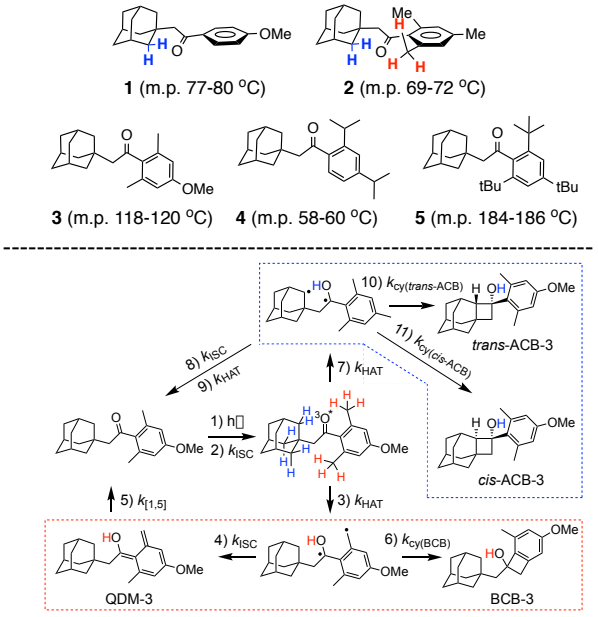

Figure 1. (Top) Structures and melting points of adamantylacetophenone derivatives, including adamantyl-*para*-methoxy-acetophenone **1** with abstractable secondary hydrogen atoms highlighted in blue and adamantyl-2,4,6-trimethylacetophenone **2** with abstractable primary benzylic hydrogens in red. (Bottom) Photochemical reaction mechanism for adamantyl-4-methoxy-2,6-dimethyl-acetophenone **3**. Colored boxes highlight reaction pathways available upon abstraction of one of the two types of γ-hydrogen atoms from the T_1 state of the ketone.

ergent hydrogen atom transfer (HAT) pathways potentially leading to Yang cyclizations and photoenolization reactions. Ketone **5** was selected to explore the competition for hydrogen abstraction between secondary adamantyl γ-hydrogens and the primary δ-hydrogens of the *ortho*-*tert*-butyl groups.

A general mechanistic scheme for these compounds is shown in the bottom part of Figure 1 with adamantyl-4-methoxy-2,6-dimethylacetophenone **3** as a representative example. The reaction starts by electronic excitation and intersystem crossing (ISC) to the T_1 state (steps 1, 2 in Figure 1) and is followed by HAT from either a benzylic position (step 3), to yield a biradical species corresponding to the triplet excited state of *ortho*-quinonedimethide QDM-**3**, or from the adamantyl methylene hydrogens (step 7) to yield a triplet 1,4-ketyl-adamantyl biradical. If HAT occurs from the adamantyl group, ISC and reverse HAT (steps 8, 9) lead back to ketone **3**. Alternatively, recombination of the biradical (steps 10, 11) can form photoproducts *trans*-ACB-**3** (*trans* referring to the relative positions of the adamantane and aromatic group with respect to the cyclobutanol ring, and ACB meaning adamantane cyclobutanol), or *cis*-ACB-**3** depending on the orientation of the radicals upon recombination. If HAT occurs from the benzylic position (step 3), intersystem crossing and radical recombination yields the benzocyclobutanol photoproduct BCB-**3** (step 6). However, ISC can also form the *ortho*-quinonedimethide QDM-**3** (step 4), which is subject to facile [1,5]-sigmatropic shift to reform ketone **3** (step 5). In the case of ketone **5**, HAT competition would occur between the secondary adamantyl γ-hydrogens and the primary δ-hydrogens of the *tert*-butyl groups. A detailed product analysis in solution and in the solid state, combined with LFP experiments of nanocrystalline suspensions of ketones **2**-**5**, revealed the feasibility of engineering competing reactions in crystals.

RESULTS AND DISCUSSION

Synthesis and Characterization. Ketones **1**, **2**, and **4** were synthesized via Friedel-Crafts acylation of the appropriate aromatic compounds with 1-adamantylacetyl chloride. Interestingly, **4** was the product isolated from the reaction with 1,4-diisopropylbenzene. A control experiment in which the acid chloride was excluded showed that the isomerization of 1,4-diisopropylbenzene occurs in the presence of aluminum chloride, as previously documented under similar conditions.[8] Therefore, the formation of **4** likely proceeds following the *in situ* isomerization of 1,4-diisopropylbenzene to 1,3-diisopropylbenzene, rather than as a result of a 1,2-isopropyl shift during reaction with the acid chloride.

Analogous conditions for the preparation of **3** failed due to regiospecific acylation occurring *ortho* to the methoxy group of the 1-methoxy-3,5-dimethylbenzene reactant. Also, since *ipso* substitution was observed for the reaction involving 1,4-di-*tert*-butylbenzene, it was assumed that **5** could also not be prepared by this method. Thus, ketones **3** and **5** were prepared by treatment of 1-adamantylacetyl chloride with the aryllithium species generated from the corresponding aryl bromide. Acetophenone derivatives **1**-**5** were isolated as colorless crystals with melting points well above room temperature as noted in Figure 1. Detailed synthetic procedures for the preparation of **1**-**5** are reported in the experimental section along with full characterization data. Their ^{1}H NMR, ^{13}C{^{1}H} NMR, UV-Vis, and IR spectra can be found in the supporting information (SI) section.

Single Crystal X-Ray Diffraction Analysis. While the lower bond dissociation energy (BDE) of the benzylic C-H bonds relative to the secondary C-H bonds of the adamantyl group may suggest that step 3 should predominate over step 7, one should expect the selectivity of the initial HAT step to also be dependent on crystal conformation. Crystals of each ketone were obtained by slow evaporation of ethanol solutions. Single crystal X-ray diffraction analysis with ketones **2**-**4** was successful and selected crystallographic parameters for each of these structures are shown in Table S2 along with data from **1**, which had been previously reported.[7] Crystals of **5** prepared in this way displayed significant twinning. Despite attempts with many different crystallization methods and solvent mixtures, samples of **5** only yielded polycrystalline material that was not amenable to X-ray diffraction.

The similarity between the molecular structures **2** and **3** extends to their crystal packing. As shown in Table S2, both crystallize in the $P\bar{1}$ space group and have similar unit cell lengths and angles. The crystal structures of ketones **1** and **4** feature greater numbers of molecules per unit cell with a corresponding increase in the length of at least one unit cell dimension.

The molecular conformation of each ketone in the crystalline solid state are shown in Figure 2. Again, the similarity of **2** and **3** manifests in nearly identical conformations with the carbonyl group almost completely perpendicular to the plane of the aromatic ring as indicated by dihedral angles of 81.6° and 85.2°, respectively. Interestingly, the carbonyl group in **4** is rotated toward the *ortho*-isopropyl group despite the potential to achieve coplanarity with the aromatic ring (as in **1**) if it were to be rotated in the opposite direction where there is a hydrogen atom. The dihedral angles between the plane of the carbonyl and the plane of the aromatic groups are 0.5° and 43.0° in ketones **1** and **4**, respectively.

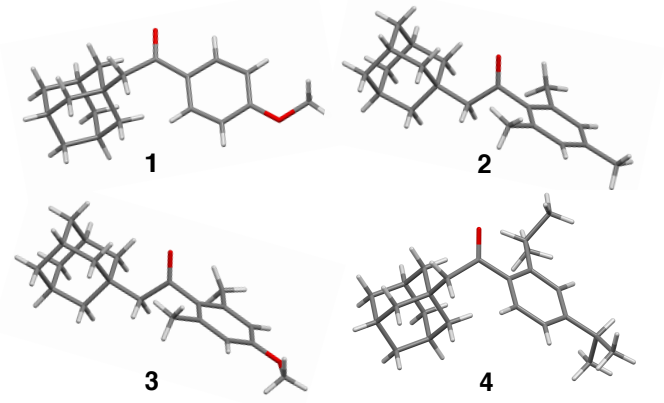

Figure 2. Molecular conformations of ketones **1**-**4** in the crystalline solid state as determined by SCXRD.

Our group has previously shown that the product selectivity of **1** is complicated by the ability of the adamantane groups to rotate in the solid state, such that the position of the adamantyl radical center can vary to give rise to the formation of products *cis*- and *trans*-ACB-**1**. Similar to the

crystal packing of **1**, the SCXRD structure of ketones **2** and **3** have the adamantane and aromatic groups form alternating layers in the crystal lattice, as shown for ketone **2** in the top part of Figure 3. Crystals of ketone **4**, however, contain only 1-dimensional chains of adamantane groups (Figure 3, bottom). While this arrangement may not eliminate the ability of the adamantane groups to rotate in the solid state, it is likely that the rotational rate would be reduced, with possible implications for reaction selectivity.

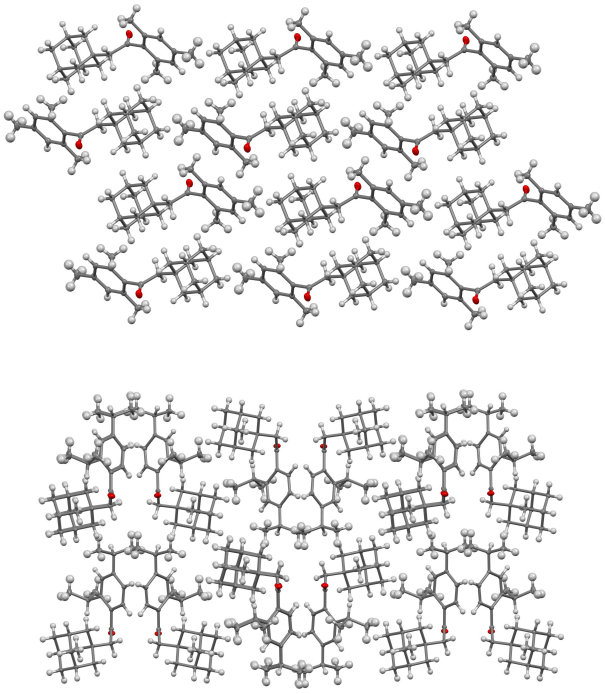

Figure 3. (Top) Crystal packing of **2** viewed down the a-axis with alternating layers of aromatic and adamantane groups. (Bottom) Crystal packing of **4** with alternating one dimensional chains of adamantane and aromatic groups generated by translation down the a-axis.

Solid State Reaction Geometry. A set of descriptors relating the ideal geometric parameters describing the position of γ-hydrogen (γH) atoms with respect to the carbonyl n-orbital involved in Norrish Type II reactivity have been developed by Scheffer.[6,9–12] These include the distance between the carbonyl carbon and the γ carbon (D), the distance between the carbonyl oxygen and the γH (d), the C=O···γH angle (Δ), the γCH···O angle (Θ), and the angular displacement of the γH from the plane of the carbonyl group (ω). The ideal values for these geometric parameters as well as those determined for ketones **1-4** based on SCXRD can be found in Table 1. Geometric parameters for ketone **5** were obtained from a calculated lowest energy structure obtained from a molecular mechanics (MMFF) conformer distribution followed by DFT calculation of its equilibrium geometry using the B3LYP functional and 6-31G* basis set. Since **1** is known to undergo Norrish-Yang cyclization in the solid state, it is apparent that these bond angles and distances may deviate significantly from their ideal values in a substrate that exhibits its photochemical reactivity. For ketones **2-4**, one would expect that hydrogen atom abstraction would take place from the γH with the geometric parameters closer to the ideal values. For derivatives **2-4** in Table 1, all of the parameters show a consistent preference for either benzylic (Benz) or adamantyl (Adam) hydrogen abstraction, with the adamantyl hydrogens being favored in **2** and **3**, and the benzylic hydrogen being favored in **4**. However, this analysis based solely on the geometric parameters incorrectly predicts the photoproducts in each case as will be shown. Also, **5** exhibits no photochemical reactivity in solution or the solid state, despite the calculated structure giving geometric parameters that indicate that hydrogen abstraction should be possible. All of these results suggest that there are additional factors to consider when predicting the outcome of this set of solid state Norrish Type II reactions.

Table 1. Geometric parameters relating carbonyl group and nearest gamma hydrogens in ketones 1-5.

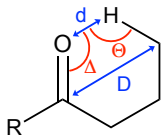

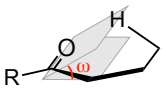

Ketone	H-Type	D [Å]	d [Å]	Δ [°]	Θ [°]	ω [°]
Ideal	γ	N/A	<2.7	90-120	180	0
1	Adam	3.015	2.651	79.12	107.94	64.39
2	Benz	2.895	2.811	76.67	110.95	61.92
	Adam	3.201	2.504	97.16	120.95	22.21
3	Benz	2.926	2.786	70.67	120.93	68.54
	Adam	3.157	2.455	96.75	121.89	26.03
4	Benz	3.067	2.354	86.88	122.32	52.17
	Adam	3.031	3.005	64.78	106.00	73.82
5[a]	δ[b]	2.894	2.409	91.93	110.85	69.81
	Adam	3.241	2.536	97.03	118.35	31.12

[a]Geometric parameters for **5** were determined from the lowest energy conformer minimized with the B3LYP/6-31G* method (SI). [b]The hydrogen atoms of the *tert*-butyl groups of **5** are δ hydrogens. Geometric parameters are measured in an analogous manner.

Nanocrystalline Suspensions. Solid state samples for transient absorption spectroscopy were prepared via the reprecipitation method.[13] Generally, this method involves dissolving the compound of interest in a water miscible organic solvent followed by rapid injection or dropwise addition of the resulting solution into vortexing water. The insolubility of the compound in the water causes instantaneous precipitation, while the motion of the water distributes the material such that the particle size is limited. The use of a dilute aqueous surfactant solution in the place of pure water is often necessary; the surfactant molecules passivate the surface of the particles once formed in order to limit aggregation. With appropriate conditions (stock solution concentration, surfactant type and concentration, addition method and vol-

ume, etc.), stable suspensions of crystalline particles with average size in the sub-micron regime can be prepared. We term such mixtures *nanocrystalline suspensions*, which have been shown to be amenable to spectroscopic analysis using standard solution-phase methods.[7,14–19] For each derivative, nanocrystalline suspensions were prepared using 0.04 mM CTAB surfactant solution and stock solutions in acetonitrile. For ketone **4**, 0.2 mL of a 2.5 mg/mL acetonitrile solution was added dropwise to ~20 mL of vortexing surfactant solution. SEM imaging (Figure 4) of a dried droplet of this suspension indicated that the particles were crystalline and exhibited a size distribution in agreement with dynamic light scattering (DLS) results. Figure 4 also contains a set of UV-Vis spectra for this suspension at several time points, along with an equimolar (0.025 mg/mL) solution of **4** in acetonitrile. As expected, the spectral features of the solution and solid state samples are identical. Despite the equivalent concentrations, the suspension spectra have a higher apparent absorbance due to Rayleigh scattering, which is proportional to $1/\lambda^4$. The similarity of the suspension spectrum over a 30-minute time period indicates that the suspension is stable (i.e. not prone to significant aggregation or decomposition) on the timescale of the transient absorption experiments.

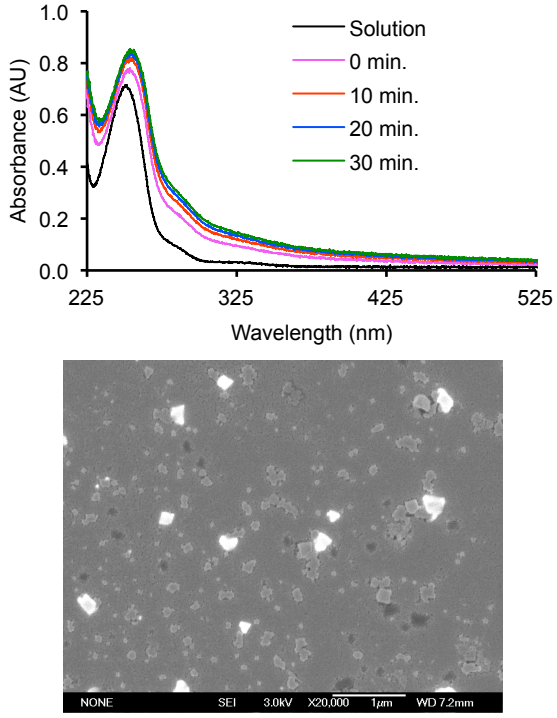

Figure 4. (Top) UV-Vis spectrum of equimolar MeCN solution and nanocrystalline suspension (several time points) of **4**. The consistency of the absorption spectrum for the suspension sample is indicative of its stability over the timeframe of the transient absorption experiments. (Bottom) SEM image of a nanocrystalline suspension of **4**. The crystal sizes were consistent with size distribution determined by DLS (232 ± 112 nm).

Lastly, an aqueous suspension of **4** with higher loading (1.0 mL of a 10.0 mg/mL solution injected into 3.0 mL of water) was dried under an air stream. The resulting powder was analyzed by powder x-ray diffraction (PXRD). The PXRD pattern matched that of the bulk powder and the simulated pattern from the SCXRD structure of **4** (Figure 5). The higher loading of suspensions for PXRD analysis is necessitated by the difficulty of collecting enough material from the dilute suspensions used for transient absorption spectroscopy. It is assumed that the crystals in each suspension share the same polymorph due to the similarity of the environments during the crystallization process. Additional SEM images of the suspension of **4** along with UV-VIS (solution and suspension), SEM, and PXRD data for suspensions of the other derivatives can be found in the SI.

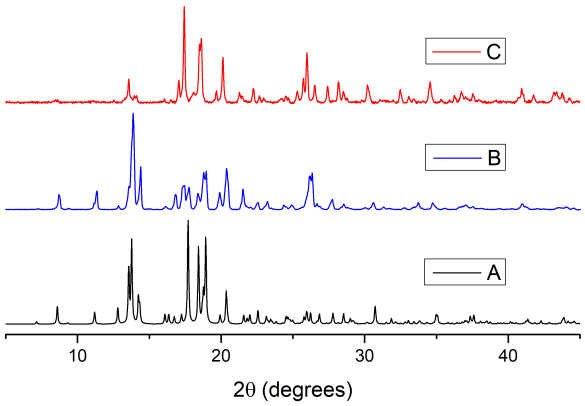

Figure 5. Powder X-ray diffraction (PXRD) of **4** (A) simulated from single crystal XRD structure, (B) bulk powder, (C) powder from dried aqueous suspension.

Solution and Solid State Photochemistry. Ketones **1-5** were subjected to irradiation with a medium pressure mercury lamp in both deuterated acetonitrile and in aqueous suspensions. The solution for **1** was prepared with 5.0 mg/mL concentration, and the remaining solutions were made such that all solutions were equimolar. Aqueous suspensions were prepared by injecting 0.1 mL of acetonitrile stock solution into 0.9 mL vortexing Millipore water. Stock solution concentrations were controlled such that the total amount of each ketone in the suspensions matched that of the solution samples. All samples were sparged with argon, then sealed in NMR tubes and irradiated simultaneously for 10 minutes and 2 hours, with ^{1}H NMR spectra being taken after each irradiation time period. Product distribution percentages for the 2-hour time point in Table 2 represent relative NMR yields of recognizable photoproducts (ignoring minor or unassignable side products) as determined by comparison to spectra of the isolated photoproducts or by inference following the isolation of the dehydrated alcohol photoproducts. Further discussion of photoproduct identification can be found in the experimental section.

Results for the 10-minute time point (SI, Table S1) exhibit a larger conversion of **1** relative to those of all other derivatives. For **2**, **3**, and **4**, the limited conversion is likely due to the favorable but unproductive reaction pathway to reform the starting material after formation of the photoenol QDM (Figure 2, steps 1-5). For **2** and **3**, this pathway was shown to be operating in solution by irradiation of solutions in 9:1 MeCN-d_3 : D_2O with concentrations that match those of the previously discussed product analysis experiments. The enol

Table 2. Photoproduct distributions of 1-4 in MeCN solutions and aqueous nanocrystalline suspensions.[a]

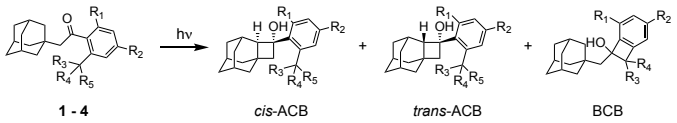

Ketone	R_1 (o)	R_2 (p)	R_3	R_4	R_5	Medium	% Conversion	% *cis*-ACB	% *trans*-ACB	% BCB	% Deuteration
1	H	OMe	N/A	N/A	N/A	MeCN	96	38	62	N/A	N/A
						Suspension	72	69	31	N/A	N/A
2	Me	Me	H	H	H	MeCN	26	0	0	100	13
						Suspension	43	0	0	100	N/A
3	Me	OMe	H	H	H	MeCN	21	16	21	63	26
						Suspension	22	13	49	37	N/A
4	H	^{i}Pr	Me	Me	H	MeCN	6	70	30	0	58[b]
						Suspension	6	78	22	0	N/A

[a]All samples were prepared as degassed MeCN-d_3 solutions or aqueous suspensions (all equimolar) and irradiated for 120 minutes with a 450 W medium pressure mercury lamp. Values in the final column (% Deuteration) are derived from an analogous set of experiments with a 9:1 MeCN-d_3 : D_2O solvent mixture. [b]Benzylic deuteration percentage for ketone **4** after 120 minutes irradiation in 8:1:1 MeCN-d_3 : D_2O : TFA-*d*. No benzylic deuteration of ketone **4** was observed when irradiated in 9:1 MeCN-d_3 : D_2O.

hydrogen of the QDM is able to exchange with deuterons from the D_2O, and after step 5 the exchanged deuterium atom replaces a hydrogen on the methyl groups *ortho* to the ketone. Multiple cycles of this reaction pathway for an individual ketone molecule results in partial or complete deuteration of these benzylic positions. Percent deuteration values (determined by ^{1}H NMR) of recovered starting material following 2 hours of irradiation of these samples are shown in Table 2. Figure 6 represents an example of the comparison of ^{1}H NMR spectra to determine these values. As noted in Table 2, deuteration of **4** was not observed under these conditions. However, modification of the solvent mixture to include an acid catalyst to promote the proton-deuterium exchange (8:1:1 MeCN-d_3 : D_2O : TFA-d) enabled deuteration of the isopropyl group. A control experiment in which an identical sample was not irradiated but allowed to stand

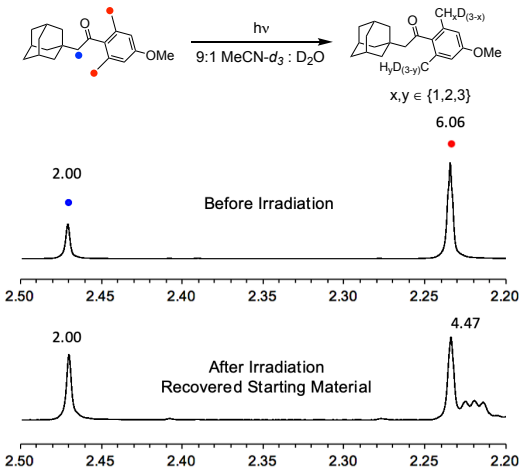

Figure 6. Partial ^{1}H NMR spectrum of **3** with labeled peaks normalized to the signal of the methylene unit before and after irradiation in a degassed 9:1 MeCN-d_3 : D_2O solution. Integration values are labeled above each peak.

for an equivalent amount of time exhibited no deuteration, ruling out a ground-state acid-catalyzed exchange mechanism (SI). Thus, it may be concluded that the formation of the QDM species as a photochemical intermediate occurs in ketones **2**, **3**, and **4**. We propose that this reaction pathway may also be active in the solid state samples and be the primary factor responsible for the reduced conversion percentages observed for both the solution and solid state samples of **2**, **3**, and **4** relative to those of **1**.

Despite the reduced conversion rate for **2**, **3**, and **4**, extended irradiation results in the formation of isolable quantities of various photoproducts. The most striking differences in reactivity are seen in ketones **2** and **4**, which exclusively form the BCB and ACB photoproducts, respectively, in both solution and aqueous suspension. In the case of mesityl derivative **2**, the selectivity for the BCB product is likely the result of a very strong preference for benzylic hydrogen abstraction (step 3) due to lower BDE value such that the biradical that would lead to the formation of the ACB photoproducts is never accessed, even in the solid state where the geometric parameters predict a preference for adamantyl hydrogen abstraction. By contrast, the deuteration experiments for the *ortho*-isopropyl ketone **4** suggest that, at least in solution, benzylic hydrogen abstraction occurs. However, the absence of any BCB-**4** in the photoproduct mixture indicates that the radical recombination (step 6) does not occur. This could be due to prohibitively large steric repulsion for the dimethyl-radical recombination, such that return back to **4** via QDM-**4** may be the only accessible pathway to this biradical. Alternatively, the formation of QDM-**4** may be fast enough to preclude any conformer that would allow radical recombination from ever being accessed. In either case, the result is that hydrogen abstraction from the adamantyl group (step 7) competes and enables the formation of the ACB photoproducts.

Interestingly, electronic excitation of adamantyl-4-methoxy-2,6-dimethylacetophenone **3** produces both ACB diastereomers as well as the BCB product. This implies that

Table 3. Phosphorescence lifetimes and preexponential factors of ketones 1-5 at 77 K in methylcyclohexane glasses.

Ketone	A_1[a]	τ_1 (ms)[a]	A_2[b]	τ_2 (ms)[b]	τ_{Ave} (ms)[c]	R^2
1	0.56	13.6	0.44	38.4	31	0.99995
2	0.98	0.51	0.02	7.27	2.0	0.99770
3	0.97	0.63	0.03	12.4	5.1	0.99618
4	0.80	12.8	0.20	967	920	0.99661
5	0.57	138	0.43	1092	955	0.99897

[a]Preexponential factors and lifetimes of the short-lived components. [b]Preexponential factors and lifetimes of the long-lived components. [c]Average lifetime calculated from the equation $\tau_{Ave} = (A_1\tau_1^2 + A_2\tau_2^2) / (A_1\tau_1+A_2\tau_2)$.[20]

the various factors affecting hydrogen abstraction and radical recombination balance, such that all possible Norrish-Yang photoproducts are formed. Considering the similarity of the solid state molecular structures of ketones **2** and **3**, both with methyl groups at their *ortho*-position, the substantial difference in photoproduct selectivity is very interesting. The ability of **3** to exhibit adamantane hydrogen abstraction in solution and in the solid sate must be the result of the change in electronic structure imparted by the *p*-methoxy group. The results of transient absorption spectroscopy experiments in MeCN solution, discussed below, support this hypothesis. While the lifetime of the T_1 state of **2** was determined to be <10 ns due to the lack of an observable transient, that of **3** is 480 ± 10 ns. The substantially longer T_1 lifetime of **3** relative to that of **2** reflects a lower reactivity that arises from a greater contribution of the (π,π*) electronic configuration, as documented for a number of acetophenone and benzophenone derivatives.[21,22] The attenuated reactivity in the case of **3** appears to allow for a decrease in selectivity, as shown by the formation of products from competing hydrogen abstraction at the adamantyl and aromatic methyl groups (Table 2). However, the lack of observable transient species for both ketones in the solid state indicates that reactions in the nanocrystals are completed within the ca. 10 ns pulse.

It is also worth noting the difference in photochemical selectivity observed between the solution and solid state reactions for **3**, with BCB favored in solution and ACB favored in the solid state. In solution, the enhanced conformational freedom enables preference for the thermodynamically favored benzylic hydrogen abstraction. In the crystalline solid, however, the ACB products are formed preferentially. The geometric parameters listed in Table 1 suggest that the adamantane γH atoms are better positioned for hydrogen abstraction to occur (the carbonyl oxygen to γH distance is shorter, and all angles are closer to the ideal values). Thus, the more favorable geometry may be able to offset the thermodynamic preference for abstraction of the hydrogen atom with lower BDE in order to form the ACB diastereomers as the major photoproducts.

Ketone **5** was found to be photochemically inert under the irradiation conditions used. This was surprising considering that 2,4,6-tri-*tert*-butylacetophenone **6** has been shown to form a cyclopentanol photoproduct upon irradiation in cyclohexane.[23] This compound was synthesized and subjected to the same irradiation conditions over 72 hours with an equimolar sample of **5**. This experiment yielded an isolable quantity of the dehydrated photoproduct **7** from 2,4,6-tri-*tert*-butylacetophenone after workup (Scheme 1), but there was no observable conversion of **5** by ^{1}H NMR. Therefore, it must be the case that the steric hindrance imposed by the adamantane group prevents either the hydrogen abstraction or the radical recombination step from occurring. Unfortunately, the lack of a crystal structure of **5** prevents this hypothesis from being further investigated by an analysis of the geometry of the ground-state structure. However, if the molecular conformation in the crystal matches that of the calculated structure of **5** (SI), then the geometric parameters in Table 1 predict that hydrogen abstraction should be possible, supporting the hypothesis that steric effects are responsible for the lack of photochemical reactivity.

Scheme 1

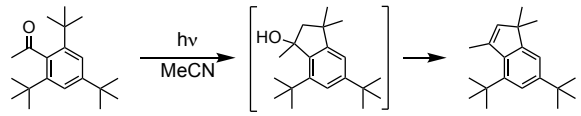

6 **7**

Irradiation of ketone **6** in acetonitrile solution results in Norrish-Yang cyclization. Compound **7** was isolated after dehydration of the native photoproduct.

Phosphorescence Spectroscopy. The phosphorescence spectra of ketones **1**-**5** were acquired at 77 K in methylcyclohexane glasses (Figures S36-S40). The emission onset in each spectrum shows that all derivatives display similar triplet energies (73.3-74.7 kcal/mol). However, the spectral features observed for **4** and **5** indicate an excited state configuration with mixed (n,π*) and (π,π*) character, while the spectra for **1**, **2**, and **3** exhibit a vibrational resolution that is typical of triplet ketones with a dominant (n,π*) configuration. This qualitative analysis is supported by complex phosphorescence lifetime data, which could be fit well by a double exponential function with short- and long-lived components as indicated in Table 3. Also included in the table are the weighted average lifetimes for each ketone, which were shown to range from ca. 2 ms and 5 ms in the cases of ketone **2** and **3**, to almost 1 s in the case of ketones **4** and **5**. The results in Table 3 indicate that the T_1 states of all of the derivatives studied here have some (π,π*) character or that states with the two configurations are close in energy.[24,25,26] The dominant nature of the short-lived (n,π*) state in the case of ketones **2** and **3** is interesting considering that they do have strong electron donating substituents in their aromatic rings. This observation may be the result of a relative-

ly poor conjugation in their corresponding aromatic carbonyls, which have dihedral angles of 81.6° and 85.2°, respectively. By comparison, the dihedral angle between the plane of the carbonyl and the plane of the aromatic group in the case of **1** and **4** is 0.5° and 43.0°, respectively.

Transient Spectroscopy and Kinetics. Experiments were conducted for each acetophenone derivative in both acetonitrile solution and in nanocrystalline suspensions using an LP 920 laser flash photolysis instrument from Edinburgh Instruments modified with a one pass flow system using a Quantel Brilliant b Nd:YAG laser with 266 nm output from two sequential second harmonic generation modules. The results for all LFP experiments are summarized in Table 4. Representative transient absorption spectra obtained for a solution of **3** and a nanocrystalline suspension of **4** are shown in Figure 7 and Figure 8, respectively. All other transient absorption spectra that were acquired can be found in Figures S69-S73. Some samples did not yield any observable transient signal (fields labeled "N/A" in Table 4), suggesting lifetimes that are shorter than the 10 ns pulse. Alternatively, the transient species may not be generated in high enough concentrations to be detectable. For solid state samples, missing data points could also be the result of poor suspension quality (e.g., crystals that are too large, fast aggregation, etc.). However, suspension characterization studies, including DLS or SEM such as that shown in Figure 4 for samples of each derivative (Figures S59-S63), help rule out this explanation. With the exception of ketone **5**, which contained crystals of significantly larger average size, all suspensions were amenable to transient absorption analysis.

Table 4. Absorption maxima and lifetimes of transient species in MeCN solution and nanocrystalline suspension.[a]

Ketone	MeCN Solution		Nanocrystalline Suspension	
	λ_{max} (nm)	Lifetime (ns)	λ_{max} (nm)	Lifetime (ns)
1	390	65 ± 2	400	810 ± 20
2	N/A	N/A	N/A	N/A
3	360	480 ± 10	N/A	N/A
4	N/A	N/A	390	1050 ± 40
5	330	740 ± 50	N/A	N/A

[a]All experiments were performed in triplicate. Lifetime values correspond to the average of the three measurements, and error ranges are reported as the sample standard deviation.

As an example, a 0.02 mg/mL solution of **3** in acetonitrile was degassed by sparging with argon for 30 minutes, then continuously pumped through the LFP flow-cell. The spectrum shown in Figure 7 was acquired, with a λ_{max} at 360 nm and a lifetime of τ = 480 ± 10 ns. This transient was assigned to the T_1 state of the ketone due to its similarity to previously documented transients of this type,[27–32] and the observation that the lifetime is reduced as a function of increasing oxygen concentration. Furthermore, considering that ketone **3** yields products arising from hydrogen abstraction from the

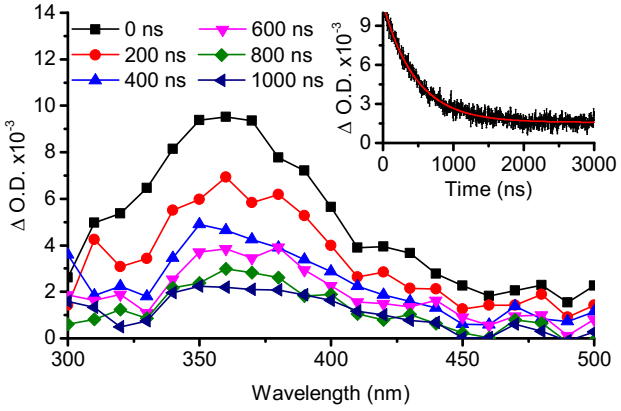

Figure 7. Transient absorption spectrum of **3** (4-methoxy-2,6-dimethyl ketone) in MeCN solution. The signal with λ_{max} = 360 nm was assigned to the T_1 state and shows a monoexponential decay (inset) with τ = 480 ± 10 ns.

adamantyl and the *ortho*-methyl groups, which proceed through two different biradicals, it is reasonable to assign the observed transient to their common precursor. This assignment implies that biradicals in solution do not accumulate, but proceed rapidly towards product formation. Analogous observations with the other ketone transients in solution led us to assign all of them to the corresponding T_1 states.

The nanocrystalline suspension of the di-isopropyl ketone **4** used for LFP experiments was identical to that used for characterization by UV-Vis, DLS, and SEM. The transient absorption spectrum acquired from its suspension is shown in Figure 8. It exhibited a λ_{max} at 390 nm with a relatively long-lived monoexponential decay rate of τ = 1050 ± 40 ns. The lack of an observable transient for this compound in solution was attributed to rapid reactivity on the timescale of the laser pulse, such that neither the T_1 state of the ketone nor the subsequent adamantyl biradicals can be detected in solution. This interpretation implies that the lifetime of the T_1 state of **4** is extended by at least two orders of magnitude from solution to the solid state, which is a more drastic example of the behavior observed between solution and suspension samples of ketone **1** (Figure S69 and S70), where

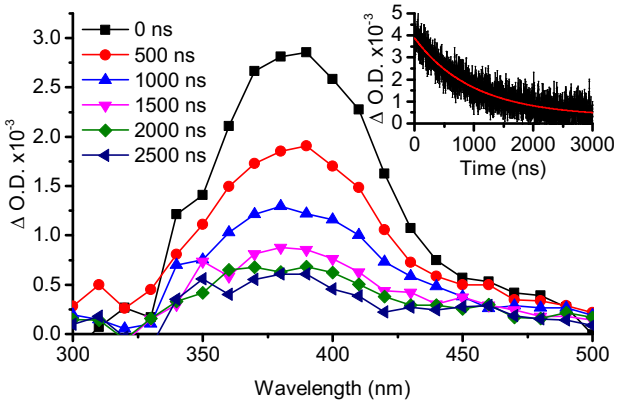

Figure 8. Transient absorption spectrum of **4** (2,4-diisopropyl ketone) in nanocrystalline suspension. The signal with λ_{max} = 390 nm was assigned to the T_1 state and shows a monoexponential decay (inset) with τ = 1050 ± 40 ns.

the conformational restrictions imposed by the crystal lattice attenuates the rate of hydrogen transfer from the triplet excited state.[6]

CONCLUSION

Nanocrystalline suspensions enabled the acquisition of the first solid state transient absorption spectrum of a compound featuring competing photochemical reaction pathways. While the lack of observable transients for other suspension samples prevented a quantitative comparison of reaction rates in the solid state, other mechanistic experiments and product analysis helped to elucidate important details about selectivity factors for the Norrish Type II reaction. It was shown that when multiple Norrish-Yang photoproducts are possible for a given substrate, many factors may affect the reaction outcome. First, the HAT selectivity is determined by geometric relationships between the carbonyl group and γH atoms, the BDEs of the γH C-H bonds, and the T_1 lifetime of the ketone. Then, the radical recombination step is influenced by conformational freedom of the biradical and the steric effects associated with the approach of the biradical toward recombination. If any of these factors is omitted from consideration, then it is not possible to account for the photoproduct distributions observed across all of the samples. Therefore, it is necessary for all of them to be included in the general framework for predicting outcomes of the Norrish Type II reaction.

EXPERIMENTAL SECTION

General Remarks. Unless noted otherwise, all reagents were used as received without further purification. Tetrahydrofuran was distilled from sodium with benzophenone indicator. Dichloromethane was distilled from calcium hydride. Acetonitrile, N,N-dimethylformamide, and methylcyclohexane were used as received. All reactions were carried out in oven-dried or flame-dried glassware under argon atmosphere. ^{1}H and ^{13}C{^{1}H} NMR spectra for characterization of synthetic targets and isolated photoproducts were acquired on a Bruker Avance spectrometer at 500 MHz (^{1}H) and 126 MHz (^{13}C{^{1}H}). ^{1}H NMR spectra of photochemical reaction product mixtures were acquired on a Bruker Avance spectrometer at 400 MHz. All chemical shifts are reported in ppm on the δ-scale relative to the residual solvent signal as reference ($CDCl_3$ δ 7.26 and δ 77.16 for proton and carbon, respectively, CD_3CN δ 1.94 for proton and δ 118.26 for carbon). Coupling constants (*J*) are reported in hertz (Hz). High-resolution mass spectrum data was recorded on a Q Exactive Plus Hybrid Quadrupole-Orbitrap Mass Spectrometer in positive ion mode. Melting point values were recorded on a Melt-Point II apparatus. Infrared spectra were recorded on a PerkinElmer Spectrum 100 spectrometer equipped with a single reflectance diamond crystal universal ATR sampling accessory. UV-Vis absorption spectra were recorded on an Ocean Optics Flame-T spectrometer with the OceanView software package. Dynamic Light Scattering (DLS) data was collected using a Beckman-Coulter N4 Plus particle analyzer. Powder X-ray diffraction patterns were measured using a Panalytical X'Pert Pro X-ray Powder Diffractometer. Single crystal X-ray diffraction data was collected on a Bruker Smart ApexII CCD-single crystal X-ray Diffractometer. Nanosecond transient absorption experiments were performed using an Edinburgh Instruments LP920 laser flash photolysis spectrometer in conjunction with a Q-switched Nd:YAG Brilliant b laser from Quantel with 266 nm output wavelength, 5–8 ns pulse width, 1 Hz repetition rate, and 36–40 mJ pulse energy. Transient absorption detection is based on a 450 W pulsed Xenon arc lamp, a Czerny-Turner TMS300 monochromator, a Hamamatsu R928 photomultiplier detector, and a Tektronix TDS3012C digital oscilloscope. Transient absorption data was collected using the L900 software package provided by Edinburgh Instruments, then processed with Origin. Laser flash photolysis samples were pumped through a 1 cm quartz flow cell mounted on a custom-built sample holder at a rate of 2 mL/min with a Masterflex L/S peristaltic pump. Samples for scanning electron microscopy (SEM) were deposited on silicon substrates and sputter-coated with gold using a Hummer 6.2 sputtering system. Samples were sputtered for 2 min., giving a ~10 nm thick gold coating according to manufacturer specifications. SEM samples were imaged using a JEOL JSM-6700F FE-SEM instrument. Phosphorescence spectra were recorded using an Edinburgh Instruments FLSP920 fluorimeter with a μF 920H microsecond flashlamp emission source. Sample irradiation for photoproduct analysis experiments was performed in a photochemical reactor with a Hanovia 450 W medium pressure mercury vapor lamp seated in a quartz immersion well. Molecular mechanics and DFT calculations were performed using the Spartan '16 program.

General preparation of nanocrystalline suspensions. Nanocrystalline suspensions of **1-5** were prepared by addition of an acetonitrile stock solution of the ketone into 0.04 mM cetyltrimethylammonium bromide (CTAB) in water such that the final mixture contained 1% acetonitrile by volume and the indicated concentration of the ketone.

2-(adamantan-1-yl)-1-(4-methoxyphenyl)ethan-1-one (1): Synthesis of **1** was conducted as previously reported with minor modifications.[7] A 50 mL round-bottom flask was charged with 1-adamantaneacetic acid (777 mg, 4.0 mmol), dry DCM (16 mL), and DMF (10 drops). The solution was stirred for 5 min., then oxalyl chloride (0.85 mL, 10.0 mmol) was added dropwise over the course of 3 min. The solution was stirred at room temperature for 1 hr., then the solvent was removed to give the acid chloride as a pale yellow oil, which was dissolved in 16 mL dry DCM and placed in an ice bath. Aluminum trichloride (1.07 g, 8.0 mmol) was added and the suspension was stirred for 10 min., followed by dropwise addition of anisole (0.87 mL, 8.0 mmol). The reaction mixture was stirred for 5 minutes at 0 °C and 90 minutes at room temp, then poured into a 0.1 M HCl solution at 0 °C. The mixture was extracted with DCM, dried over $MgSO_4$, and the solvent was removed. The crude product was purified by column chromatography (SiO_2, 9:1 hexanes : ethyl ether). Recrystallization from ethanol gave the product as a white, crystalline solid (713 mg, 63 %). R_f = 0.38 (9:1 hexanes : ethyl acetate). m.p. 77-80 °C (lit.[1] 80-81 °C). IR (powder): 2896, 1653, 1591, 1508, 1454, 1312, 1256, 1174, 1144, 1017, 843, 821, 781, 770, 581, 535 cm^{-1}. ^{1}H NMR (500 MHz, $CDCl_3$): δ 7.94 (d, *J* = 9.0 Hz, 2H), 6.92 (d, *J* = 9.0 Hz, 2H), 3.87 (s, 3H), 2.66 (s, 2H), 1.94 (br s, 3H), 1.65 (m, 12H) ppm. ^{13}C{^{1}H} NMR (126 MHz, $CDCl_3$): δ 199.0, 163.4, 132.2, 130.9, 113.7, 55.6, 51.2, 43.2, 36.9, 34.1, 28.9

ppm. HRMS (APCI, quadrupole-orbitrap) m/z: $[M+H]^+$ calculated for $C_{19}H_{25}O_2$: 285.1849, found: 285.1838.

2-(adamantan-1-yl)-1-mesitylethan-1-one (2): An equivalent amount of the acid chloride solution as described in the synthesis of **1** was prepared in an identical manner. Aluminum trichloride (1.07 g, 8.0 mmol) was added and the suspension was stirred for 10 min. Mesitylene (1.11 mL, 8.0 mmol) was added dropwise and the mixture was stirred for 1 hr. at 0 °C and 90 min. at room temperature. The reaction mixture was poured into ice cold 0.1 M HCl solution, extracted with DCM, washed with brine, dried over $MgSO_4$, and evaporated to give the crude product as a yellow oil. The crude product was purified by column chromatography (SiO_2, 4 : 1 hexanes : DCM). The resulting clear oil was crystallized from cold hexanes to give **2** as a white, crystalline solid (828 mg, 70% yield). R_f = 0.58 (9:1 hexanes : ethyl acetate). m.p. 69–72 °C. IR (film): 2879, 2845, 1694, 1612, 1449, 1336, 1212, 1149, 998, 980, 910, 850, 601, 526 cm^{-1}. ^1H NMR (500 MHz, $CDCl_3$): δ 6.81 (s, 2H), 2.47 (s, 2H), 2.26 (s, 3H), 2.21 (s, 6H), 1.98 (br s, 3H), 1.75 (m, 12H) ppm. $^{13}C\{^1H\}$ NMR (126 MHz, $CDCl_3$): δ 209.7, 140.6, 138.1, 132.5, 128.7, 57.6, 42.2, 37.1, 33.3, 28.8, 21.2, 19.2 ppm. HRMS (APCI, quadrupole-orbitrap) m/z: $[M+H]^+$ calculated for $C_{21}H_{29}O$: 297.2213, found: 297.2212.

2-bromo-5-methoxy-1,3-dimethylbenzene (8): Synthesis of **8** was conducted as previously reported.[33] A 100 mL round-bottom flask was charged with 1-methoxy-3,5-dimethylbenzene (2.83 mL, 20.0 mmol) and MeCN (20 mL). The flask was placed on an ice bath. A solution of N-bromosuccinimide (3.92 g, 22.0 mmol) in MeCN (30 mL) was transferred to an addition funnel and added to the flask over 10 min. The reaction was stirred at 0 °C for 2 hrs., then poured into 100 mL H_2O and extracted with hexanes. The organic layers were dried over $MgSO_4$ and evaporated to give **8** as a pale yellow oil without further purification (3.78 g, 88% yield). R_f = 0.72 (hexanes). IR (film): 2953, 1586, 1468, 1408, 1320, 1195, 1162, 1077, 1018, 998, 853, 614 cm^{-1}. ^1H NMR (500 MHz, $CDCl_3$): δ 6.65 (s, 2H), 3.76 (s, 3H), 2.39 (s, 6H) ppm. $^{13}C\{^1H\}$ NMR (126 MHz, $CDCl_3$): δ 158.2, 139.2, 118.4, 114.0, 55.5, 24.2 ppm. HRMS (APCI, quadrupole-orbitrap) m/z: $[M]^+$ calculated for $C_9H_{11}BrO$: 213.9988, found: 213.9986.

2-(adamantan-1-yl)-1-(4-methoxy-2,6-dimethylphenyl)-ethan-1-one (3): A 10 mL round-bottom flask was charged with 1-adamantaneacetic acid (194 mg, 1.0 mmol). Dry DCM (4 mL) and DMF (2 drops) were added, followed by dropwise addition of oxalyl chloride (0.21 mL, 2.5 mmol). The solution was stirred at room temperature for 2 hrs., then the solvent was removed. A second 10 mL round-bottom flask was charged with **8** (215 mg, 1.0 mmol) and dry THF (2 mL), then cooled to -78 °C and charged with t-butyllithium solution (1.2 mL, 1.7 M in pentane). The mixture was stirred for 1 hr. at -78 °C, then allowed to warm to room temperature. Dry THF (2 mL) was added to the acid chloride, which was then cooled to -78 °C. The aryllithium solution was then transferred by syringe to the acid chloride solution over the course of 5 min. The reaction was stirred for 70 min. at -78 °C, and 100 min. at room temperature. Then, the mixture was quenched with H_2O, extracted with DCM, dried over $MgSO_4$, and evaporated to give the crude product as a dark orange oil (246 mg). The crude product was purified by flash chromatography (SiO_2, 39 : 1 hexanes : ethyl acetate) and recrystallization from ethanol to give **3** as a white, crystalline solid (45 mg, 14% yield). R_f = 0.48 (9:1 hexanes : Ethyl Acetate). m.p. 118–120 °C. IR (film): 2901, 2848, 1700, 1605, 1451, 1338, 1316, 1192, 1146, 982, 838, 551 cm^{-1}. ^1H NMR (500 MHz, $CDCl_3$): δ 6.52 (s, 2H), 3.77 (s, 3H), 2.47 (s, 2H), 2.23 (s, 6H), 1.97 (br s, 3H), 1.73 (m, 12H) ppm. $^{13}C\{^1H\}$ NMR (126 MHz, $CDCl_3$): δ 209.4, 159.3, 136.4, 134.6, 113.3, 58.0, 55.3, 42.3, 37.1, 33.5, 28.8, 19.8 ppm. HRMS (APCI, quadrupole-orbitrap) m/z: $[M]^+$ calculated for $C_{21}H_{28}O_2$: 312.2084, found: 312.2088.

2-(adamantan-1-yl)-1-(2,4-diisopropylphenyl)ethan-1-one (4): An equivalent amount of the acid chloride solution as described in the synthesis of **1** was prepared in an identical manner. Aluminum trichloride (1.07 g, 8.0 mmol) was added and the suspension was stirred for 10 min. 1,4-diisopropylbenzene (1.51 mL, 8.0 mmol) was added dropwise and the mixture was stirred for 2 hrs. at 0 °C and 90 min. at room temperature. The reaction mixture was poured into ice cold 0.1 M HCl solution, extracted with DCM, washed with brine, dried over $MgSO_4$, and evaporated to give the crude product as a golden oil. The crude product was purified by column chromatography (SiO_2, 4 : 1 hexanes : DCM). The resulting yellow oil was crystallized from cold hexanes to give **4** as a white, crystalline solid (542 mg, 40% yield). R_f = 0.58 (9:1 hexanes : ethyl acetate). m.p. 58–60 °C. IR (film): 2966, 2901, 2844, 1663, 1605, 1447, 1303, 1283, 1255, 1062, 1017, 973, 846, 697, 600 cm^{-1}. ^1H NMR (500 MHz, $CDCl_3$): δ 7.36 (d, J = 8.0 Hz), 7.23 (d, J = 1.6 Hz, 1H), 7.05 (dd, J = 8.0, 1.6 Hz, 1H) , 3.39 (sept, J = 6.8 Hz, 1H), 2.91 (sept, J = 6.9 Hz, 1H) 2.64 (s, 2H), 1.94 (br s, 3H), 1.66 (m, 12H), 1.25 (d, J = 6.9 Hz, 6H), 1.24 (d, J = 6.8 Hz, 6H) ppm. $^{13}C\{^1H\}$ NMR (126 MHz, $CDCl_3$): δ 206.2, 151.7, 147.7, 138.8, 127.9, 125.0, 123.1, 56.0, 43.0, 37.0, 34.3, 34.3, 29.5, 28.8, 24.5, 23.9 ppm. HRMS (APCI, quadrupole-orbitrap) m/z: $[M+H]^+$ calculated for $C_{24}H_{35}O$: 339.2682, found: 339.2681.

2-bromo-1,3,5-tri-*tert*-butylbenzene (9): Synthesis of **9** was conducted as previously reported.[34] A 100 mL round bottom flask with a reflux condenser was charged with 1,3,5-tri-*tert*-butylbenzene (4.00 g, 16.2 mmol). Trimethyl phosphate (40 mL, 342 mmol) was added and the mixture was heated to 70 °C. Bromine (1.66 mL, 32.5 mmol) was added and the reaction was stirred at 70 °C for 26 hrs. The reaction mixture was allowed to cool to room temperature, and the orange suspension was poured into aqueous sodium thiosulfate solution (100 mL, 10% w/v) then extracted with hexanes. The organic layer was dried over $MgSO_4$ and evaporated to give a yellow solid. Recrystallization from ethanol gave **9** as a pale yellow, crystalline solid (3.164 g, 69% yield). R_f = 0.72 (hexanes). m.p. 169-171 °C (lit.[3] 167-169 °C). IR (powder): 2956, 1590, 1475,1396, 1362, 1241, 1216, 1011, 877, 739, 578 cm^{-1}. ^1H NMR (500 MHz, $CDCl_3$): δ 7.41 (s, 2H), 1.59 (s, 18H), 1.32 (s, 9H) ppm. $^{13}C\{^1H\}$ NMR (126 MHz, $CDCl_3$): δ 148.7, 148.6, 123.8, 121.8, 38.5, 35.1, 31.5, 31.1 ppm. HRMS (APCI, quadrupole-orbitrap) m/z: $[M]^+$ calculated for $C_{18}H_{29}Br$: 324.1447, found: 324.1447.

2-(adamantan-1-yl)-1-(2,4,6-tri-*tert*-butylphenyl)ethan-1-one (5): A 50 mL round-bottom flask was charged with 1-adamantaneacetic acid (597 mg, 3.07 mmol), DCM (10 mL), and DMF (4 drops). Oxalyl chloride (0.66 mL, 7.7 mmol)

was added dropwise to the solution, which was then stirred for 1 hr. The solvent was removed and the resulting residue was redissolved in 10 mL THF. A 25 mL round-bottom flask was charged with **9** (1.0 g, 3.07 mmol) and THF (10 mL), then placed in a dry ice / acetone bath. The solution was treated with n-butyllithium (2.5 mL, 2.5 M in hexanes) and allowed to stir for 30 min. before warming to room temperature. Meanwhile, the acid chloride solution was placed in a dry ice / acetone bath. Once the solution aryllithium solution had reached room temp., it was transferred to the acid chloride solution dropwise via syringe, and the resulting mixture was stirred for 3 hrs. Then, the reaction mixture was poured into 0.1 M HCl, extracted with DCM, dried over $MgSO_4$ and evaporated to give the crude product as a brown oil. Upon standing overnight, crystals had grown from the oil. The crystals were washed with ethanol, then dissolved in DCM and dried to give 133 mg off-white solid, which was passed through a silica plug with hexanes as eluent then dried to give **5** as a white, crystalline solid (75 mg, 6% yield). R_f = 0.75 (9:1 hexanes : ethyl acetate). m.p. 184–186 °C. IR (film): 2963, 2902, 2848, 1703, 1601, 1454, 1393, 1363, 1332, 1195, 978, 909, 731, 650 cm^{-1}. ^1H NMR (500 MHz, $CDCl_3$): δ 7.35 (s, 2H), 2.62 (s, 2H), 1.98 (br s, 3H), 1.82 (br s, 6H), 1.72 (br s, 6H), 1.39 (s, 18H), 1.31 (s, 9H) ppm. $^{13}C\{^1H\}$ NMR (126 MHz, $CDCl_3$): δ 210.5, 149.0, 145.2, 137.6, 123.1, 60.8, 42.3, 37.8, 37.2, 34.9, 33.5, 33.4, 31.4, 28.8 ppm. HRMS (APCI, quadrupole-orbitrap) m/z: $[M+H]^+$ calculated for $C_{30}H_{47}O$: 423.3621, found: 423.3615.

2,4,6-tri-tert-butylbenzoic acid (10): Synthesis of **10** was conducted as previously reported with minor modifications.[23] A 50 mL round-bottom flask was charged with **9** (1.00 g, 3.07 mmol). THF (20 mL) was added and the flask was cooled to -78 °C, then the solution was treated with n-butyllithium (1.23 mL, 2.5 M in hexanes) and stirred for 30 min. Dry CO_2 was then bubbled through the solution for 10 min., with the cold bath being removed after the first 5 min. The reaction mixture was poured into a solution of 50 mL H_2O and 2 mL 2 M HCl, extracted with DCM, dried over $MgSO_4$ and evaporated to give the crude product as a white solid, which was purified by flash chromatography (SiO_2, 4:1 hexanes : ethyl acetate) to give **10** as a white powder (871 mg, 97% yield). R_f = 0.0.35 (4:1 hexanes : ethyl acetate). m.p. 292-294 °C (lit.[4] 291-293 °C). IR (film): 2959, 1694, 1603, 1459, 1390, 1363, 1287, 1218, 1165, 1083, 909, 878, 745 cm^{-1}. ^1H NMR (500 MHz, $CDCl_3$): δ 7.45 (s, 2H), 1.49 (s, 18H), 1.33 (s, 9H) ppm. $^{13}C\{^1H\}$ NMR (126 MHz, $CDCl_3$): δ 180.3, 150.9, 146.5, 127.7, 122.3, 37.2, 35.2, 32.4, 31.4 ppm. HRMS (APCI, quadrupole-orbitrap) m/z: $[M+H]^+$ calculated for $C_{19}H_{31}O_2$: 291.2319, found: 291.2308.

1-(2,4,6-tri-tert-butylphenyl)ethan-1-one (6): A 35 mL round-bottom flask was charged with **10** (200 mg, 0.69 mmol), DCM (10 mL), and DMF (1 drop). Oxalyl chloride (0.15 mL, 1.72 mmol) was added and the mixture (heterogeneous at the beginning due to limited solubility of **10** in DCM) was stirred for 1 hr. The solvent was removed and the resulting yellow solid was redissolved in 10 mL THF. The flask was cooled to 0 °C and 0.46 mL 3 M MeMgBr solution in diethyl ether was added. After 45 min., the reaction mixture was poured into 10 mL 0.1 M HCl solution, extracted with DCM, dried over $MgSO_4$, and evaporated to give the crude product as a white solid, which was purified by flash chromatography (SiO_2, 49:1 hexanes : ethyl acetate) and recrystallization from methanol to give **6** as a white solid (30 mg, 15% yield). R_f = 0.35 (19:1 hexanes : ethyl acetate). m.p. 110-116 °C (lit.[4] 120.5-122 °C). IR (film): 2961, 1699, 1602, 1465, 1396, 1363, 1350, 1246, 1217, 1148, 879 cm^{-1}. ^1H NMR (500 MHz, $CDCl_3$): δ 7.39 (s, 2H), 2.64 (s, 3H), 1.38 (s, 18H), 1.32 (s, 9H) ppm. $^{13}C\{^1H\}$ NMR (126 MHz, $CDCl_3$): δ 211.9, 149.5, 144.7 137.7, 122.9, 38.4, 37.3, 35.0, 33.1, 31.4 ppm. HRMS (APCI, quadrupole-orbitrap) m/z: $[M]^+$ calculated for $C_{20}H_{32}O$: 288.2448, found: 288.2451.

4,6-di-*tert*-butyl-1,1,3-trimethyl-1*H*-indene (7): A 20 mL screw-cap vial was charged with 15 mg **6** and 15 mL MeCN. The solution was sparged with argon for 10 minutes, then the vial was sealed with parafilm. The solution was irradiated in the Hanovia photochemical reactor for 72 hours, then the solvent was removed. Upon dissolving the resulting solid in $CDCl_3$, a significant change in TLC results indicated that the $CDCl_3$ promoted dehydration of the cyclopentanol photoproduct to form **7**, presumably due to trace HCl. Preparatory TLC with hexanes as eluent enabled isolation of **7** as a white solid (2.4 mg, 17% yield). R_f = 0.32 (hexanes). m.p. 102-104 °C. IR (film): 2955, 2865, 1610, 1458, 1396, 1362, 1253, 960, 875, 815 cm^{-1}. ^1H NMR (500 MHz, $CDCl_3$): δ 7.36 (d, *J* = 2.0 Hz, 1H), 7.20 (d, J = 2.0 Hz, 1H), 6.12 (q, *J* = 1.38 Hz, 1H), 2.44 (d, *J* = 1.43 Hz, 3H), 1.54 (s, 2H), 1.50 (s, 9H), 1.36 (s, 9H), 1.25 (s, 6H) ppm. $^{13}C\{^1H\}$ NMR (126 MHz, $CDCl_3$): δ 157.1, 147.1, 146.9, 144.6, 138.0, 136.1, 121.5, 116.5, 46.1 35.4, 34.9, 33.3, 31.7, 25.4, 21.1 ppm. HRMS (APCI, quadrupole-orbitrap) m/z: $[M+H]^+$ calculated for $C_{20}H_{31}$: 271.2420, found: 271.2426.

General photoproduct isolation and photoproduct distribution determination. Photoproducts were isolated by preparative TLC with 49:1 or 19:1 hexanes : ethyl acetate as eluent. The photoproducts of ketones **1** and **2** were isolated in their native form (*trans*-ACB-**1**, *cis*-ACB-**1**, and BCB-**2**). However, cyclobutanols from ketones **3** and **4** transformed into corresponding alkenes by water elimination upon chromatographic purification. In the case of ketone **4**, a correlation of ^1H NMR spectra before and after purification showed that *trans*-ACB-**4** is isolated as the H_2O elimination product but *cis*-ACB-**4** can be obtained in its native form. For ketone **3**, only the elimination products were isolated. Relative percentages of *trans*-ACB-**3**, cis-ACB-**3**, and BCB-**3** were determined from crude ^1H NMR spectra by integration of the distinctive cyclobutanol methine proton of *cis*-ACB-**3** at δ 2.90, the methoxy protons of *trans*-ACB-**3** at δ 3.72, and the cyclobutanol methylene protons of BCB-**3** at δ 3.42 and δ 2.99. In all cases, relative percentages of photoproducts as well as conversion percentages were determined by integration of characteristic signals of the starting material and photoproducts in the crude ^1H NMR spectra. Product distributions determined from this analysis for **1-5** after 10 minutes and 2 hours of irradiation in both MeCN solutions and aqueous suspensions are shown in Table S1.

***trans*-ACB-1**: ^1H NMR (500 MHz, $CDCl_3$): δ 7.36 (d, *J* = 8.8 Hz, 2H), 6.90 (d, *J* = 8.8 Hz, 2H), 3.82 (s, 3H), 2.70 (d, *J* = 10.9 Hz, 1H), 2.62 (br s, 1H), 2.38 (br s, 1H), 2.06 (d, *J* = 11.2 Hz, 1H), 1.99 (m, 1H), 1.81 (m, 5H), 1.59 (m, 3H), 1.50 (m, 2H), 1.39 (m, 2H) ppm. $^{13}C\{^1H\}$ NMR (126 MHz, $CDCl_3$): δ 159.1, 136.2, 129.2, 113.9, 81.7, 60.1, 55.4, 47.7, 45.9, 41.2, 38.1, 37.7, 30.91, 30.89, 29.9, 29.0, 28.3 ppm.

HRMS (APCI, quadrupole-orbitrap) m/z: $[M+H]^+$ calculated for $C_{19}H_{25}O_2$: 285.1849, found: 285.1839.

***cis*-ACB-1**: ^{1}H NMR (500 MHz, $CDCl_3$): δ 7.26 (d, *J* = 8.8 Hz, 2H), 6.87 (d, *J* = 8.8 Hz, 2H), 3.80 (s, 3H), 2.91 (m, 1H), 2.36 (br s, 1H), 2.31 (m, 1H), 2.25 (d, *J* = 11.1 Hz, 1H), 2.20 (m, 1H), 2.11 (d, *J* = 11.1 Hz, 1H), 2.02 (m, 2H), 1.75 (m, 8H), 1.64 (s, 1H) ppm. $^{13}C\{^1H\}$ NMR (126 MHz, $CDCl_3$): δ 158.7, 142.0, 126.3, 113.9, 84.1, 55.49, 55.47, 48.5, 45.6, 41.2, 39.8, 38.3, 34.1, 32.4, 31.2, 30.1, 28.7 ppm. HRMS (APCI, quadrupole-orbitrap) m/z: $[M+H]^+$ calculated for $C_{19}H_{25}O_2$: 285.1849, found: 285.1838.

BCB-2: ^{1}H NMR (500 MHz, $CDCl_3$): δ 6.80 (s, 1H), 6.78 (s, 1H), 3.56 (d, *J* = 14.3 Hz, 1H), 3.10 (d, *J* = 14.3 Hz, 1H), 2.30 (s, 3H), 2.27 (s, 3H), 2.02 (m, 2H), 1.96 (m, 3H), 1.85 (m, 3H), 1.69 (m, 9H), 1.53 (d, *J* = 14.7 Hz, 1H) ppm. $^{13}C\{^1H\}$ NMR (126 MHz, $CDCl_3$): δ 147.2, 141.5, 139.2, 131.6, 129.3, 121.6, 81.6, 50.8, 48.0, 43.8, 37.2, 34.3, 29.0, 22.1, 16.9 ppm. HRMS (APCI, quadrupole-orbitrap) m/z: $[M+H]^+$ calculated for $C_{21}H_{29}O$: 297.2213, found: 297.2201.

Elimination product of *cis*- and *trans*-ACB-3: ^{1}H NMR (500 MHz, $CDCl_3$): δ 6.57 (s, 2H), 3.77 (s, 3H), 2.47 (m, 3H), 2.31 (m, 6H), 2.09 (m, 2H), 2.00 (m, 2H), 1.85 (m, 2H), 1.75 (m, 6H) ppm. $^{13}C\{^1H\}$ NMR (126 MHz, $CDCl_3$): δ 157.8, 156.2, 138.2, 128.7, 122.1, 112.6, 55.1, 46.0, 43.1, 39.2, 37.0, 36.8, 31.5, 29.9, 21.1 ppm. HRMS (APCI, quadrupole-orbitrap) m/z: $[M]^+$ calculated for $C_{21}H_{26}O$: 294.1978, found: 297.1972.

Elimination product of BCB-3: ^{1}H NMR (500 MHz, $CDCl_3$): δ 6.57 (s, 1H), 6.52 (s, 1H), 5.35 (s, 1H), 3.77 (s, 3H), 3.66 (s, 2H), 2.28 (s, 3H), 2.00 (m, 3H), 1.76 (m, 6H), 1.71 (m, 6H) ppm. $^{13}C\{^1H\}$ NMR (126 MHz, $CDCl_3$): δ 159.7, 146.0, 137.5, 133.9, 131.5, 128.7, 115.0, 105.3, 55.5, 42.9, 38.3, 36.9, 36.1, 28.6, 18.1 ppm. HRMS (APCI, quadrupole-orbitrap) m/z: $[M]^+$ calculated for $C_{21}H_{26}O$: 294.1978, found: 297.1989.

Elimination product of *trans*-ACB-4: ^{1}H NMR (500 MHz, $CDCl_3$): δ 7.20 (d, *J* = 8.0 Hz, 1H), 7.12 (d, *J* = 1.7 Hz, 1H), 7.01 (dd, *J* = 8.0, 1.7 Hz, 1H), 3.38 (sept, *J* = 6.9 Hz, 1H), 2.87 (sept, *J* = 6.9 Hz, 1H), 2.85 (m, 1H), 2.57 (s, 2H), 2.08 (m, 2H), 1.97 (m, 2H), 1.89 (m, 2H), 1.78 (m, 4H), 1.69 (m, 2H), 1.24 (d, *J* = 6.9 Hz, 6H), 1.23 (d, *J* = 6.9 Hz, 6H) ppm. $^{13}C\{^1H\}$ NMR (126 MHz, $CDCl_3$): δ 154.3, 147.2, 145.6, 132.6, 128.2, 123.3, 123.2, 123.1, 45.1, 42.7, 38.7, 37.3, 36.7, 34.1, 32.5, 29.7, 29.2, 24.0, 23.9 ppm. HRMS (APCI, quadrupole-orbitrap) m/z: $[M]^+$ calculated for $C_{24}H_{32}$: 320.2499, found: 320.2493.

***cis*-ACB-4**: ^{1}H NMR (500 MHz, $CDCl_3$): δ 7.17 (d, *J* = 1.9 Hz, 1H), 7.15 (d, *J* = 7.9 Hz, 1H), 7.00 (dd, *J* = 7.9, 1.9 Hz, 1H), 3.37 (sept, *J* = 6.9 Hz, 1H), 2.93 (m, 1H), 2.88 (sept, *J* = 6.9 Hz, 1H), 2.49 (s, 1H), 2.38 (br s, 1H), 2.33 (d, *J* = 11.1 Hz, 1H), 2.29 (d, *J* = 11.1 Hz, 1H), 2.20 (m, 1H), 2.02 (m, 2H), 1.82 (m, 2H), 1.73 (m, 6H), 1.67 (br s, 1H), 1.25 (d, *J* = 6.9 Hz, 6H), 1.21 (d, *J* = 6.9 Hz, 6H) ppm. $^{13}C\{^1H\}$ NMR (126 MHz, $CDCl_3$): δ 148.2, 147.5, 142.9, 125.7, 125.1, 123.2, 85.1, 54.9, 49.9, 45.5, 41.0, 39.6, 38.1, 34.4, 33.9, 32.2, 30.9, 30.6, 28.7, 28.5, 24.7, 24.5, 24.02, 23.99 ppm. HRMS (APCI, quadrupole-orbitrap) m/z: $[M+H]^+$ calculated for $C_{24}H_{35}O$: 339.2682, found: 339.2693.

ASSOCIATED CONTENT

Supporting Information

Spectroscopic ^{1}H NMR and $^{13}C\{^1H\}$ NMR for all new compounds and IR data compounds **1**-**10**. Phosphorescence, UV-Vis and transient absorption data along with characterization of suspensions by DLS, SEM and PXRD for compounds **1**-**5**. Photoproduct distributions percentages for compounds **1**-**5** and photochemical deuteration experiments for compounds **2**-**4**. Single crystal X-ray thermal ellipsoid plots and crystallography data for compounds **2**-**4**. Calculated structure of compound **5**. (PDF). Single crystal X-ray structures for compounds **2**-**4** (CIF files).

AUTHOR INFORMATION

Corresponding Author

* mgg@chem.ucla.edu

Notes

ORCID:
Miguel A. Garcia-Garibay: 0000-0002-6268-1943
Vince M. Hipwell: 0000-0001-6297-241X

ACKNOWLEDGMENT

This work was supported by grants National Science Foundation grants CHE-1855342, MRI-1532232 (solid state NMR), and CHE-1048804 (solution NMR).

REFERENCES

(1) Yang, N. C.; Yang, D. D. H. Photochemical Reactions of Ketones in Solution. *J. Am. Chem. Soc.* **1958**, *80*, 2913–2914.

(2) Leibovitch, M.; Olovsson, G.; Scheffer, J. R.; Trotter, J. An Investigation of the Yang Photocyclization Reaction in the Solid State: Asymmetric Induction Studies and Crystal Structure-Reactivity Relationships. *J. Am. Chem. Soc.* **1998**, *120*, 12755–12769.

(3) Cai, X.; Cygon, P.; Goldfuss, B.; Griesbeck, A. G.; Heckroth, H.; Fujitsuka, M.; Majima, T. α-Carbonyl Substituent Effect on the Lifetimes of Triplet 1,4-Biradicals from Norrish-Type-II Reactions. *Chem. - A Eur. J.* **2006**, *12*, 4662–4667.

(4) Cindro, N.; Halasz, I.; Mlinarič-Majerski, K.; Basarič, N. Photoinduced H-Abstraction in Homo- and Protoadamantylphthalimide Derivatives in Solution and in Organized and Constrained Media. *European J. Org. Chem.* **2013**, 929–938.

(5) Chen, C. The Past, Present, and Future of the Yang Reaction. *Org. Biomol. Chem.* **2016**, *14*, 8641–8647.

(6) Gudmundsdottir, A. D.; Lewis, T. J.; Randall, L. H.; Scheffer, J. R.; Rettig, S. J.; Trotter, J.; Wu, C. H. Geometric Requirements for Hydrogen Abstractability and 1,4-Biradical Reactivity in the Norrish/Yang Type II Reaction: Studies Based on the Solid State Photochemistry and X-Ray Crystallography of Medium-Sized Ring and Macrocyclic Diketones. *J. Am. Chem. Soc.* **1996**, *118*, 6167–6184.

(7) Kuzmanich, G.; Vogelsberg, C. S.; Maverick, E. F.; Netto-Ferreira, J. C.; Scaiano, J. C.; Garcia-Garibay, M. A. Reaction Mechanism in Crystalline Solids: Kinetics and Conformational Dynamics of the Norrish Type II Biradicals from α-Adamantyl- p -Methoxyacetophenone. *J. Am. Chem. Soc.* **2012**, *134*, 1115–1123.

(8) Olah, G. A.; Carlson, C. G.; Lapierre, J. C. Friedel-Crafts Isomerization. X. Aluminum Chloride Catalyzed Isomerization of the Di-t-Butylbenzenes. *J. Org. Chem.* **1964**, *29*, 2687–2689.

(9) Ihmels, H.; Scheffer, J. R. The Norrish Type II Reaction in the Crystalline State: Toward a Better Understanding of the

Geometric Requirements for γ-Hydrogen Atom Abstraction. *Tetrahedron* **1999**, *55*, 885–907.

(10) Vishnumurthy, K.; Cheung, E.; Scheffer, J. R.; Scott, C. Enhanced Regioselectivity of Yang Photocyclization in the Crystalline State. *Org. Lett.* **2002**, *4*, 1071–1073.

(11) Braga, D.; Chen, S.; Filson, H.; Maini, L.; Netherton, M. R.; Patrick, B. O.; Scheffer, J. R.; Scott, C.; Xia, W. 1,4-Hydroxybiradical Behavior Revealed through Crystal Structure-Solid-State Reactivity Correlations. *J. Am. Chem. Soc.* **2004**, *126*, 3511–3520.

(12) Turowska-Tyrk, I.; Bąkowicz, J.; Scheffer, J. R. Monitoring Structural Transformations in Crystals. 11. Yang Photocyclizations - One Type of Reaction, but Diversity of Structural Changes. *Acta Crystallogr. Sect. B Struct. Sci.* **2007**, *63*, 933–940.

(13) Nakanishi, H. K.; Hari, S. N.; Hidetoshi, O.; Shuji, O.; Hiro, M.; Nobutsugu, M.; Atsushi, K.; Katsumichi, O.; Akio, M.; Hachiro. A Novel Preparation Method of Organic Microcrystals. *Jpn. J. Appl. Phys.* **1992**, *31*, L1132.

(14) Ayitou, A. J. L.; Flynn, K.; Jockusch, S.; Khan, S. I.; Garcia-Garibay, M. A. Structure-Kinetics Correlations in Isostructural Crystals of α-(Ortho-Tolyl)-Acetophenones: Pinning Down Electronic Effects Using Laser-Flash Photolysis in the Solid State. *J. Am. Chem. Soc.* **2016**, *138*, 2644–2648.

(15) Breslin, V. M.; Garcia-Garibay, M. A. Transmission Spectroscopy and Kinetics in Crystalline Solids Using Aqueous Nanocrystalline Suspensions: The Spiropyran-Merocyanine Photochromic System. *Cryst. Growth Des.* **2017**, *17*, 637–642.

(16) Chung, T. S.; Ayitou, A. J. L.; Park, J. H.; Breslin, V. M.; Garcia-Garibay, M. A. Photochemistry and Transmission Pump-Probe Spectroscopy of 2-Azidobiphenyls in Aqueous Nanocrystalline Suspensions: Simplified Kinetics in Crystalline Solids. *J. Phys. Chem. Lett.* **2017**, *8*, 1845–1850.

(17) Breslin, V. M.; Barbour, N. A.; Dang, D. K.; Lopez, S. A.; Garcia-Garibay, M. A. Nanosecond Laser Flash Photolysis of a 6-Nitroindolinospiropyran in Solution and in Nanocrystalline Suspension under Single Excitation Conditions. *Photochem. Photobiol. Sci.* **2018**, *17*, 741–749.

(18) Park, J. H.; Chung, T. S.; Hipwell, V. M.; Rivera, E.; Garcia-Garibay, M. A. Transient Kinetics and Quantum Yield Studies of Nanocrystalline α-Phenyl-Substituted Ketones: Sorting Out Reactions from Singlet and Triplet Excited States. *J. Am. Chem. Soc.* **2018**, *140*, 8192–8197.

(19) Chin, K. K.; Natarajan, A.; Gard, M. N.; Campos, L. M.; Shepherd, H.; Johansson, E.; Garcia-Garibay, M. A. Pump-Probe Spectroscopy and Circular Dichroism of Nanocrystalline Benzophenone - Towards Absolute Kinetic Measurements in Solid State Photochemical Reactions. *Chem. Commun.* **2007**, 4266–4268.

(20) Johnson, B. A.; Gamarnik, A.; Garcia-Garibay, M. A. Deuterium Tunneling in Triplet 5,8-Dimethyl-1-Tetralone by Phosphorescence Detection between 80 and 15 K. *J. Phys. Chem.* **2002**, *100*, 4697–4700.

(21) Wagner, P. J.; Kemppainen, A. E.; Schott, H. N. Effects of Ring Substituents on the Type II Photoreactions of Phenyl Ketones. How Interactions between Nearby Excited Triplets Affect Chemical Reactivity. *J. Am. Chem. Soc.* **1973**, *95*, 5604–5614.

(22) Wagner, P. J.; Truman, R. J.; Scaiano, J. C. Substituent Effects on Hydrogen Abstraction by Phenyl Ketone Triplets. *J. Am. Chem. Soc.* **1985**, *107*, 7093–7097.

(23) Ditto, S. R.; Card, R. J.; Davis, P. D.; Neckers, D. C. Synthesis and Photochemistry of 2,4,6-Tri-Tert-Butylacetophenone. *J. Org. Chem.* **1979**, *44*, 894–896.

(24) Griffin, R. N. Phosphorescence of Aromatic Ketones in Low-Temperature Glasses. *Photochem. Photobiol.* **1968**, *7*, 159–173.

(25) Scharf, G.; Winefordner, J. D. Phosphorescence Characteristics of Acetophenone, Benzophenone, p-Aminobenzophenone and Michlercs Ketone in Various Environments. *Talanta* **1986**, *33*, 17–25.

(26) Romani, A.; Ortica, F.; Favaro, G. Proximity Effects in the Excited State Ordering and Photophysics of Thienyl-Pyridyl Ketones. *Chem. Phys.* **1998**, *237*, 413–424.

(27) Lutz, H.; Bréhéret, E.; Lindqvist, L. Effects of Solvent and Substituents on the Absorption Spectra of Triplet Acetophenone and the Acetophenone Ketyl Radical Studied by Nanosecond Laser Photolysis. *J. Phys. Chem.* **1973**, *77*, 1758–1762.

(28) Carmichael, I.; Helman, W. P.; Hug, G. L. Extinction Coefficients of Triplet-Triplet Absorption Spectra of Organic Molecules in Condensed Phases: A Least Squares Analysis. *J. Phys. Chem. Ref. Data* **1987**, *16*, 239–260.

(29) Netto-Ferreira, J. C.; Scaiano, J. C. Effect of Cyclodextrin Complexation on the Photochemistry of p-Methoxy-β-Phenylpropiophenone. *J. Photochem. Photobiol., A* **1988**, *45*, 109–116.

(30) Wismontski-Knittel, T.; Kilp, T. Intramolecular Quenching of Carbonyl Triplets by β-Phenyl Rings. *J. Phys. Chem.* **2005**, *88*, 110–115.

(31) Samanta, S.; Mishra, B. K.; Pace, T. C. S.; Sathyamurthy, N.; Bohne, C.; Moorthy, J. N. β-Phenyl Quenching of Triplet Excited Ketones: How Critical Is the Geometry for Deactivation? *J. Org. Chem.* **2006**, *71*, 4453–4459.

(32) Wilkinson, F.; Willsher, C. J.; Casal, H. L.; Johnston, L. J.; Scaiano, J. C. Intrazeolite Photochemistry. IV. Studies of Carbonyl Photochemistry on the Hydrophobic Zeolite Silicalite Using Time-Resolved Diffuse Reflectance Techniques. *Can. J. Chem.* **2006**, *64*, 539–544.

(33) Zysman-Colman, E.; Arias, K.; Siegel, J. S. Synthesis of Arylbromides from Arenes and N -Bromosuccinimide (NBS) in Acetonitrile — A Convenient Method for Aromatic Bromination . *Can. J. Chem.* **2009**, *87*, 440–447.

(34) Knorr, R.; Pires, C.; Behringer, C.; Menke, T.; Freudenreich, J.; Rossmann, E. C.; Böhrer, P. Carbenoid Chain Reactions: Substitutions by Organolithium Compounds at Unactivated 1-Chloro-1-Alkenes. *J. Am. Chem. Soc.* **2006**, *128*, 14845–14853.

Table of Contents Graphic